Initial Characterization of an ^{18}F-Labeled Myocardial Perfusion Tracer

Marc C. Huisman[1], Takahiro Higuchi[1], Sybille Reder[1], Stephan G. Nekolla[1], Thorsten Poethko[1], Hans-Jürgen Wester[1], Sibylle I. Ziegler[1], David S. Casebier[2], Simon P. Robinson[2], and Markus Schwaiger[1]

[1]Department of Nuclear Medicine, Klinikum Rechts der Isar, Technische Universität München, Munich, Germany; and [2]Department of Discovery Chemistry and Department of Discovery Biology, Bristol Myers Squibb Medical Imaging, North Billerica, Massachusetts

PET allows for quantitative, regional myocardial perfusion imaging. The short half-lives of the perfusion tracers currently in use limit their clinical applicability. Here, the biodistribution and imaging quality of a new ^{18}F-labeled myocardial perfusion agent (^{18}F-BMS-747158-02) in an animal model are described. **Methods:** The biodistribution of ^{18}F-BMS-747158-02 was determined at 10 and 60 min after injection. The first-pass extraction fraction of the tracer was measured in isolated rat hearts perfused with the Langendorff method. Small-animal PET imaging was used to study tracer retention. **Results:** The biodistribution at 10 min after injection demonstrated high myocardial uptake (3.1 percentage injected dose per gram [%ID/g]) accompanied by little activity in the lungs (0.3 %ID/g) and liver (1.0 %ID/g). The tracer showed a high and flow-independent myocardial first-pass extraction fraction, averaging 0.94 (SD = 0.04). PET imaging provided excellent delineation of myocardial structures. The heart-to-lung activity ratio increased from 4.7 to 10.2 between 1 and 15 min after tracer injection (at rest). Adenosine infusion (140 μg/kg/min) led to a significant increase in myocardial tracer retention (from 1.68 [SD = 0.23]) s^{-1} to 3.21 [SD = 0.92] s^{-1}; $P = 0.03$). **Conclusion:** The observation of a high and flow-independent first-pass extraction fraction promises linearity between tracer uptake and myocardial blood flow. Sustained myocardial tracer uptake, combined with high image contrast, will allow for imaging protocols with tracer injection at peak exercise followed by delayed imaging. Thus, ^{18}F-BMS-747158-02 is a promising new tracer for the quantitative imaging of myocardial perfusion and can be distributed to imaging laboratories without a cyclotron.

Key Words: PET; myocardial perfusion; imaging

The assessment of myocardial blood flow during rest and stress conditions has become an important clinical tool for diagnosing coronary artery stenosis in patients with suspected ischemic heart disease (*1,2*). PET allows for the quantification of regional myocardial blood flow (*3,4*). Attenuation

correction provides accurate delineation of regional tracer kinetics, which are used in combination with validated tracer kinetic models to quantify myocardial perfusion in mL/min/g of tissue (*5,6*). Recently, the combination of PET and CT offered the opportunity to develop a comprehensive cardiac examination including an assessment of coronary calcification, CT angiography, and quantitation of the myocardial perfusion reserve (*7*). Anatomic and functional information will provide a unique characterization of coronary artery disease (CAD), assessing the severity of stenosis and providing a prognosis with one imaging approach.

At present, several blood flow tracers are available for use with PET. The availability of these blood flow tracers depends on local production either by a cyclotron facility in close proximity or by a generator, as in the case of ^{82}Rb. This limitation has restricted the application of PET flow measurements. Therefore, the need for an ^{18}F-labeled flow tracer is well appreciated. Such a tracer can be distributed as a single-dose unit in a fashion similar to that of ^{18}F-FDG or ^{99m}Tc-labeled flow tracers, widening the application of PET perfusion imaging.

Recently, the first ^{18}F-labeled radiopharmaceutical for the assessment of myocardial perfusion was proposed (*8*), underscoring the interest in such a tracer. The purpose of the present study was to characterize a new ^{18}F-radiolabeled PET perfusion tracer (^{18}F-BMS-747158-02) in a rat model. ^{18}F-BMS-747158-02 is a pyridazinone analog designed to target mitochondrial complex I of the electron transport chain with high affinity. Uptake into the heart is selective because of the high density of mitochondria in myocardial tissue. In addition to biodistribution, the in vivo pharmacokinetics in the rat myocardium as well as surrounding tissues were measured by dynamic small-animal PET imaging. Studies with perfused isolated rat hearts were used to determine the first-pass myocardial extraction fraction of this tracer at different flow rates.

MATERIALS AND METHODS

Animal Studies

All animal studies were performed with healthy mature male Wistar rats (275 [SD = 25] g; Charles River Laboratories, Inc.). Animals were used in only one experiment, and all experiments

were performed in accordance with guidelines for the care and use of living animals in scientific studies and the German Law for the Protection of Animals.

Tracer Preparation

Dry cryptate ([K⊂2.2.2.]⁺¹⁸F⁻) was resolubilized with a solution of BMS-747155-01 in dry acetonitrile. The mixture was stirred at 90°C for 10 min. ¹⁸F-BMS-747158-02 was purified by preparative high-performance liquid chromatography. After dilution, the product fraction ¹⁸F-BMS-747158-02 was immobilized on a reversed-phase cartridge, washed, and eluted with ethanol. The solvent was removed under reduced pressure. Quality control was performed with an analytic high-performance liquid chromatography system. The entire synthesis was completed within 60 min. The overall radiochemical yield was 50%–60%, and the radiochemical purity was 99%. The value of log $P_{Oct/PBS}$ was 0.76 ± 0.01 (mean ± SD), indicating moderate lipophilicity.

Biodistribution Study

For the biodistribution study, 6.3–7.0 MBq of ¹⁸F-BMS-747158-02 in 150 μL of phosphate-buffered saline (pH 7.4) was injected into a lateral tail vein. The animals were anesthetized with isoflurane (Abbott GmbH & Co.; 1.5% by volume, 2.0 L of O_2/min) during tracer injection. The animals were awake during the uptake period of 10 min ($n = 3$) or 60 min ($n = 3$), after which they were euthanized by carbon dioxide inhalation. The organs of interest were rapidly dissected and weighed. Organ activity levels were determined by well counting with the appropriate energy window and decay correction. Data were expressed as percentage injected dose per gram (%ID/g).

Perfused Isolated Rat Heart Study

Hearts were quickly excised from anesthetized rats (intraperitoneal sodium pentobarbital [0.25 mL]; Merial GmbH), placed in ice-chilled Krebs–Henseleit bicarbonate buffer (glucose at 10 mmol/L), and cannulated via the aorta. Krebs–Henseleit buffer, oxygenated with a mixture of 95% oxygen and 5% carbon dioxide, was used to perfuse the heart (without recirculation; $n = 3$, $n = 4$, and $n = 4$ for flow velocities of 5, 8.3, and 16.6 mL/min, respectively). The heart was stabilized for a period of 15 min, after which a bolus injection of ~0.925 MBq of ¹⁸F-BMS-747158-02 (0.037 MBq/μl) was given. Whole-heart radioactivity was measured over 10 min with a pair of bismuth germanate detectors interfaced to coincidence detection circuitry. Care was taken to keep the counting rate within the linear response range of the system, to prevent dead-time–induced counting rate losses during tracer injection. The total coincidence counting rate was measured as a function of time and corrected for decay. The curve was analyzed by fitting an exponentially decaying function to the data representing the tissue washout component (from 100 s to 600 s). The fitted curve was extrapolated to the time of the maximum counting rate, and the value obtained was divided by the measured maximum counting rate. This ratio is a measure of the extraction fraction (Fig. 1; please note that for visibility, only data up to 100 s are shown, together with the extrapolated fitted curve). Because the curve was essentially linear in the fit region, possible differences between an exponential fit and a linear fit were studied. No differences were found for the determination of the extraction fraction (data not shown).

Small-Animal PET Imaging

Rats were imaged in the prone position with a dedicated animal PET scanner (microPET Focus 120; Siemens Medical Solutions)
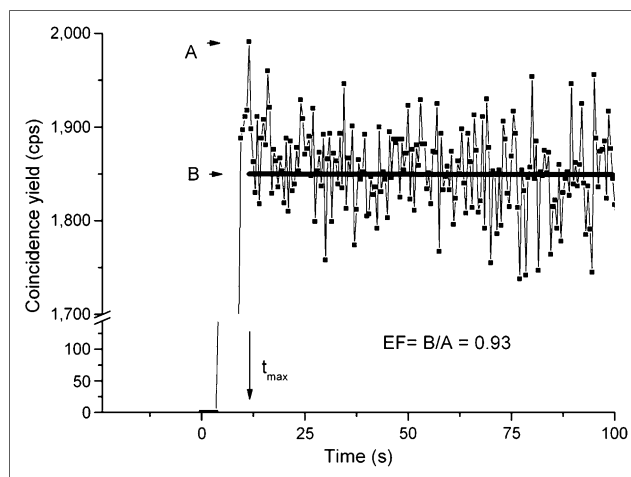
FIGURE 1. Data from first-pass extraction fraction (EF) measurements. Typical time–activity curve (for flow velocity of 8.3 mL/min) is shown, together with extrapolation of fit to tissue washout portion of curve ($100 < t$ [s] < 600; fit itself is not shown). Extraction fraction is defined as ratio of measured (A) to extrapolated (B) values at time point at which measured curve reaches its maximum value (indicated by t_{max}).

(9,10). The animals were anesthetized by the intramuscular administration of a mixture of midazolam (0.1 mg/kg), fentanyl (1.0 μg/kg), and medetomidin (10.0 μg/kg). For injection of activity, a catheter was placed in a lateral tail vein. Data acquisition started before the intravenous injection of ~37 MBq of ¹⁸F-BMS-747158-02 in 500 μL of phosphate-buffered saline (pH 7.4). To increase myocardial blood flow, we performed stress studies during the infusion of adenosine via a separate catheter placed in a different lateral tail vein (11). Adenosine (140 μg/kg/min; Sanofi-Synthelabo, GmbH) was infused over a period extending from 5 min before to 2 min after the start of the imaging procedure with an infusion pump. Measurements were obtained for 6 animals in the rest group and 6 animals in the stress group. Data were acquired in list mode format for 20 min, and histograms were used to produce a 29-frame sinogram (18×5 s, 7×30 s, 2×150 s, and 2×5 min). The sinogram was reconstructed into an image of $128 \times 128 \times 95$ voxels by use of filtered backprojection with a ramp filter with a cutoff at the Nyquist frequency. The voxel size equaled $0.433 \times 0.433 \times 0.796$ mm³, and the effective spatial resolution was less than 2.0 mm. Data were normalized and corrected for randoms, dead time, and decay.

Image Analysis

Image analysis was performed with the ASIPro software package (Siemens Medical Solutions) as well as with the Munich Heart software package (12). The latter software allows for image reorientation, enabling viewing of the heart along the short, vertical long, and horizontal long axes.

Regions of interest (ROIs) were manually defined in transaxial slices of the frame reconstructed from data measured between 15 and 20 min after injection. Blood-pool (left ventricular cavity) and myocardial ROIs were drawn on 3 contiguous slices near the basal plane of the heart. Lung and liver ROIs were drawn close to the heart. The mean activities in the ROIs (in arbitrary units, proportional to cps/mL) were plotted as a function of time (time–activity curves). These regional time–activity curves were used to determine uptake

TABLE 1
Biodistribution of ^{18}F-BMS-747158-02 in Male Wistar Rats

| Tissue | Mean (SD) %ID/g at following time after injection*: | |
	10 min	60 min
Blood	0.12 (0.01)	0.15 (0.01)
Lungs	0.32 (0.08)	0.21 (0.02)
Heart	3.07 (0.66)	2.06 (0.83)
Liver	0.99 (0.23)	0.38 (0.05)
Stomach	0.74 (0.42)	0.38 (0.07)
Spleen	0.20 (0.01)	0.15 (0.01)
Pancreas	1.01 (0.19)	0.36 (0.08)
Intestines	0.45 (0.06)	0.29 (0.01)
Kidneys	2.00 (0.42)	0.62 (0.04)
Adrenal glands	0.20 (0.04)	0.21 (0.05)
Bone	0.17 (0.03)	0.20 (0.01)
Brain	1.07 (0.28)	0.58 (0.08)
Muscle	0.17 (0.03)	0.20 (0.03)

*n = 3 per time point.

ratios for myocardium to liver, myocardium to blood, and myocardium to lung.

Tracer retention (1/s) was defined as the myocardial activity concentration divided by the integral under the input function. For calculation of tracer retention at 1 and 2 min after injection, the ROIs described earlier were used to define myocardial uptake. The time integral of the input function for 1 and 2 min was defined by fitting a γ-variate function to the measured input function. The homogeneity of myocardial tracer uptake was determined with the Munich Heart software. Polar map representations of uptake after 2 min were derived. The values in the polar map representation of the tracer indicated the percentage of mean tracer uptake in the ROI, normalized to the maximum myocardial uptake (expressed as a percentage of the maximum).

Statistical Methods

Values are reported as mean (SD). Statistical significance was tested with a standard t test.

RESULTS

Biodistribution Study

Table 1 shows the biodistribution (%ID/g) of ^{18}F-BMS-747158-02. Uptake in the heart was approximately 3 times higher than that in the liver and 10 times higher than that in lung tissue. The route of excretion of the compound was primarily renal, consistent with the observed rapid decrease in activity in the kidneys.

Perfused Isolated Rat Heart Study

Typical time–activity curves for all flow velocities are shown in Figure 2. The vascular component was very small in the time–activity curves, indicating high tracer extraction. Slow tracer washout was implied by the almost constant tissue activity during the acquisition time interval. A high and flow-independent extraction fraction was found (Table 2). The differences between the flow groups were not statistically significant ($P \geq 0.05$).

Small-Animal PET Study

One animal in the stress group moved during the scan. Therefore, the data pertaining to this animal were not useful. Thus, all data analysis was based on 6 animals in the rest group and 5 animals in the stress group.

Figure 3 shows an imaging example of the uptake of ^{18}F-BMS-747158-02 in the myocardium at 15–20 min after injection. High contrast between the myocardium and blood, lungs, and liver was seen. Right ventricular activity was delineated, indicating high extraction and retention, as well as low nonspecific binding of the tracer.

FIGURE 2. First-pass extraction fraction (EF) as function of blood flow. Smoothed time–activity curves obtained from sequential measurements of single rat heart are shown. Flow velocities and extraction fractions are indicated.

A
Flow = 5.0 mL/min
EF = 0.93

B
Flow = 8.3 mL/min
EF = 0.95

C
Flow = 16.6 mL/min
EF = 0.93
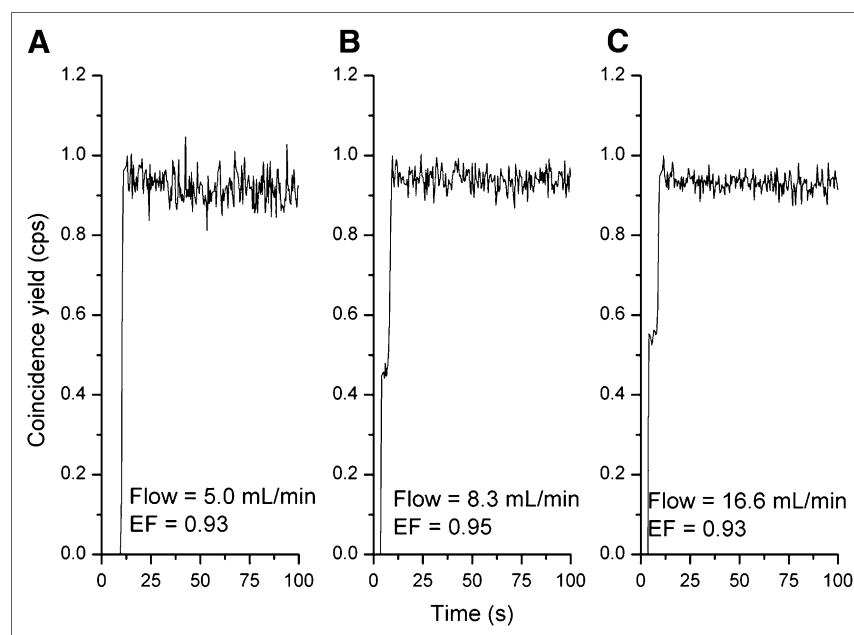
TABLE 2
Average Extraction Fractions Measured
with Langendorff Method

Flow velocity, mL/min (n)	Mean (SD) extraction fraction*
5.0 (3)	0.94 (0.04)
8.3 (4)	0.92 (0.04)
16.6 (4)	0.95 (0.03)

*Differences between groups were not significant ($P \geq 0.05$).

Figure 4 shows typical time–activity curves for the myocardium and the blood pool under rest and stress conditions, normalized to the same injected dose. The effect of adenosine infusion was clear.

The uptake ratios derived from the time–activity curves for the myocardium, liver, blood, and lungs at 1, 2, 5, and 15 min after injection are shown in Table 3. The in vivo–derived heart-to-blood and heart-to-liver activity ratios did not change for the time points analyzed, whereas the heart-to-lung activity ratio increased (from 4.7 to 10.2 between 1 and 15 min at rest). During the 20 min of data acquisition, no significant washout of the tracer from the myocardium was observed. The retention values after 1 and 2 min were 1.77 (SD = 0.30) s^{-1} and 1.68 (SD = 0.23) s^{-1} for the rest group and 3.27 (SD = 0.74) s^{-1} and 3.21 (SD = 0.92) s^{-1} for the stress group, respectively (Fig. 5). The adenosine-induced increase in tracer retention was significant ($P < 0.05$). The ratios of stress to rest values averaged 1.85 and 1.91 at 1 and 2 min after injection, respectively.

The distribution of myocardial tracer uptake at 2 min after injection was determined for myocardial wall ROIs. For the rest and stress groups, the average means were 82.4% (SD = 6.3%) and 81.9% (SD = 5.3%), respectively. Table 4 shows the mean uptake values for different left ventricular segments.

DISCUSSION

Several blood flow tracers are available for use with cardiac PET; they have been validated in animal models and clinical studies. The most physiologic tracer is ^{15}O-water, because it diffuses freely across membranes, resulting in a flow-independent myocardial extraction fraction close to 1.

However, ^{15}O-water has a physical half-life of only 120 s, limiting its application to facilities with an on-site cyclotron. In addition, the rapid washin and washout kinetics of ^{15}O-water imaging limit count statistics and compromise the regional evaluation of myocardial blood flow (6,13). Nevertheless, this tracer has gained acceptance in research laboratories for the quantification of myocardial blood flow and flow reserve in various clinical protocols (14,15).

[13]N-Ammonia is widely used as a flow tracer because of its high myocardial extraction fraction and its relatively long physical half-life (10 min), which together facilitate good image quality. Several studies have validated ^{13}N-ammonia as a marker for the qualitative as well as quantitative assessment of regional myocardial blood flow (16–18). Tracer kinetic models are used to compensate for decreasing myocardial extraction fractions at higher flows, yielding accurate measurements of flow over a wide flow range (4,5). A pattern of heterogeneous retention of ^{13}N-ammonia has been observed in healthy volunteers, limiting the specificity of perfusion defect detection, especially in the lateral wall of the left ventricle (1,4).

[82]Rb offers the advantage of being a generator-produced radiopharmaceutical with a generator shelf life of about 4 wk. The very short half-life of [82]Rb, 76 s, and the relatively low myocardial extraction fraction result in image quality very similar to that provided by ^{99m}Tc-based SPECT tracers. This tracer has been validated extensively and is being used clinically as a routine generator-produced radiopharmaceutical in the application of PET and PET/CT for the work-up of patients with CAD (19–22).

Recently, ^{18}F-labeled fluorobenzyl triphenyl phosphonium, a member of the class of potentiometric lipophilic phosphonium cations originally developed for measurement of the mitochondrial membrane potential, was introduced for myocardial perfusion imaging (8). The accumulation of the tracer depends primarily on the mitochondrial membrane potential. Furthermore, the myocardium-to-liver uptake ratio is approximately 1, hampering image contrast for myocardial structures.

In the present study, ^{18}F-BMS-747158-02 was characterized with respect to its usefulness as a PET tracer for myocardial perfusion imaging. The chemical structure of ^{18}F-BMS-747158-02 represents a modification of the pyridazinone insecticide pyridaben. These compounds act through tight binding to mitochondrial complex I, the first component

FIGURE 3. Late image (15–20 min after injection) of ^{18}F-BMS-747158-02 uptake. Transaxial, coronal, and sagittal views are shown from left to right.

FIGURE 4. PET-derived time–activity curves. (A) Time–activity curves for blood pool and myocardial (Myocard) tissue for animal in stress group. (B) Corresponding time–activity curves for animal in rest group, normalized to same injected dose. Vertical axes are in arbitrary units (a.u.), proportional to cps/mL.
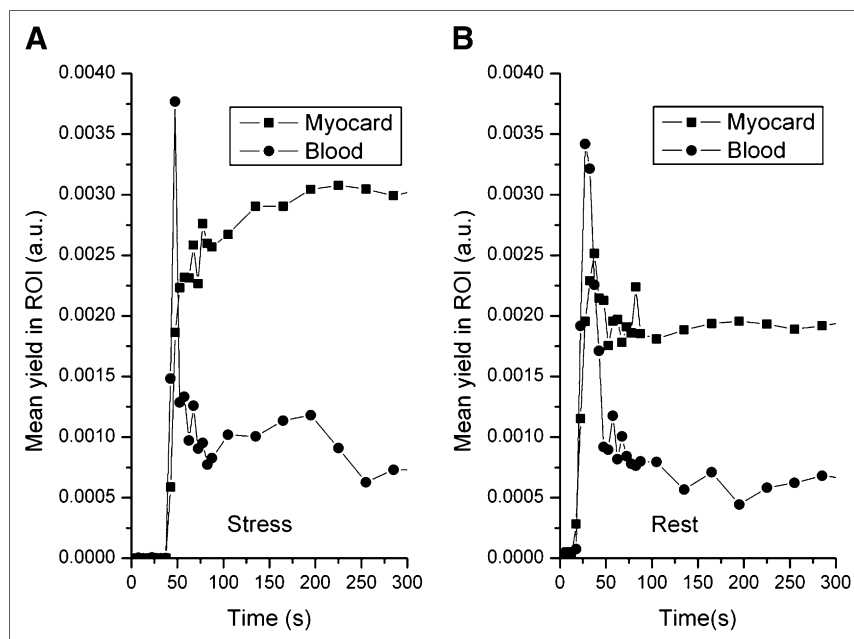
of the electron transport chain, which is highly conserved. ^{18}F-BMS-747158-02 is selectively taken up into the heart because of the high density of mitochondria in cardiac muscle (23,24). The lipophilicity of the compound and its high binding affinity (50% inhibitory concentration of ~13.8 nM (25)) result in a very high binding capacity.

Our study of the first-pass extraction fraction of the tracer in an isolated rat heart showed that the extraction fraction was higher than 90% and essentially flow independent (5–15 mL/min). Therefore, we conclude that delivery of the tracer by myocardial flow remains the limiting factor for retention, fulfilling the requirement for an almost ideal flow tracer.

This high extraction fraction is surprising, because the flow rates in the non–blood-perfused rat heart are considerably higher than those under physiologic conditions. Other common SPECT and PET perfusion tracers that are retained in the myocardium have considerably lower values. The SPECT tracer ^{99m}Tc-sestamibi has an average myocardial extraction fraction of 0.38 (SD = 0.09) for a flow range of 0.52–3.19 mL/min/g (26). For ^{13}N-ammonia, an extraction fraction of 0.82 (SD = 0.06) has been found at a control flow after injection into the left circumflex coronary artery (27); lower extraction fractions have been found at higher flows (in mL/min/100 g; calculated as extraction fraction = $1 - 0.607^{-125/\text{flow}}$). For [82]Rb, a value of 0.42 (SD = 0.06) has been found after injection into the femoral vein at normal resting flow rates (0.75–1.5 mL/min/g) (28). The observation of an essentially flow-independent extraction fraction for ^{18}F-BMS-747158-02 implies a linear relationship between uptake and myocardial blood flow, which is an important attribute for stress flow measurements. To our knowledge, the observed increase in tracer retention in the rat heart during pharmacologic stress testing with adenosine infusion is the first documentation of the expected relationship between uptake and perfusion. The stress-to-rest retention ratio of approximately 1.9 in the present study corresponds well to the reported value of 1.8 (SD = 0.6) for adenosine stress testing with validated tracer kinetic models of ^{13}N-ammonia in the rat heart (11). However, further studies with larger animals and labeled microspheres as a gold standard are

TABLE 3
In Vivo–Derived Uptake Ratios for ^{18}F-BMS-747158-02 in Male Wistar Rats

Group (n)	Ratio	Mean (SD) uptake ratio at the following time after injection:			
		1 min	2 min	10 min	15 min
Rest (6)	Myocardium to liver	2.49 (1.05)	2.13 (0.82)	2.17 (0.74)	2.40 (0.78)
	Myocardium to blood	4.60 (2.14)	4.36 (1.70)	4.53 (1.02)	4.59 (0.97)
	Myocardium to lungs	4.66 (1.28)	5.94 (1.89)	9.79 (1.92)	10.16 (1.93)
Stress (5)	Myocardium to liver	2.65 (0.26)	2.40 (0.33)	2.80 (0.55)	3.09 (0.68)
	Myocardium to blood	3.53 (0.76)*	4.38 (1.99)*	5.07 (0.88)	5.19 (1.09)
	Myocardium to lungs	6.06 (2.22)	8.22 (2.34)	12.35 (1.73)	12.73 (1.84)

*Blood data used were averages of 3 data points closest to time indicated.
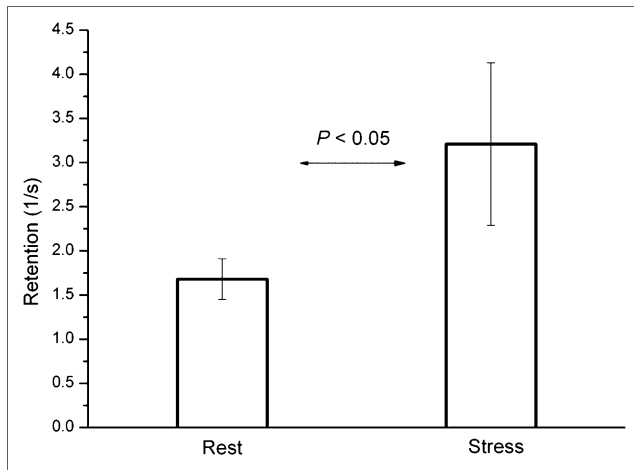
FIGURE 5. Retention values at rest and stress. Retention values determined after 1 min under rest and stress conditions indicated significant increase in blood flow during adenosine infusion. Vertical lines indicate SDs.

being performed in our laboratory to define the relationship between ^{18}F-BMS-747158-02 PET flow measurements and microsphere-derived blood flow in the heart (*29*).

Because this tracer is bound to mitochondrial structures, it needs to be clarified whether alterations in the metabolic state of the myocardium (hypoxia or ischemia) affect the regional retention of the tracer. Such alterations have been observed with ^{99m}Tc-sestamibi, which is also retained in mitochondrial structures (*30*). However, small metabolically induced changes in tissue retention may not affect the overall diagnostic performance of an imaging approach, as shown by blood flow data obtained with [99m]Tc.

The metabolic fate of the tracer was not evaluated in the present study. An observed slight increase in blood activity over time (Table 1) may suggest the presence of metabolites with different tissue uptake characteristics. Therefore, tracer retention estimates were restricted to the first 2 min after tracer injection, when metabolic effects are expected to be negligible.

The relatively slow washout of the tracer allows for imaging protocols with high count statistics. Gated data acquisition would provide measurements of ventricular volumes and wall motion. Patients can be injected during peak

TABLE 4
Distribution of ^{18}F-BMS-747158-02 Uptake
at 120 Seconds After Injection

Location	Mean (SD) % uptake for the following group:	
	Rest ($n = 6$)	Stress ($n = 5$)
Anterior	90.4 (6.9)	89.4 (4.2)
Septal	82.5 (10.0)	87.1 (7.7)
Inferior	77.1 (8.8)	74.8 (8.7)
Lateral	78.0 (7.8)	83.6 (10.4)
Apical	81.7 (12.3)	77.3 (12.0)

exercise on a treadmill and transferred for imaging after the completion of the exercise protocol.

CONCLUSION

The data presented here describe a promising ^{18}F-labeled perfusion tracer which, in combination with PET/CT, can be clinically useful for a comprehensive evaluation of patients with CAD. Such an evaluation can include assessment of coronary stenosis by coronary CT angiography and quantitation of flow reserve and global and regional ventricular function by PET.

REFERENCES

1. Schwaiger M, Melin J. Cardiological applications of nuclear medicine. *Lancet.* 1999;354:661–666.
2. Hesse B, Tägil K, Cuocolo A, et al. EANM/ESC procedural guidelines for myocardial perfusion imaging in nuclear cardiology. *Eur J Nucl Med Mol Imaging.* 2005;32:855–897.
3. Schelbert HR, Wisenberg G, Phelps ME, et al. Noninvasive assessment of coronary stenoses by myocardial imaging during pharmacologic coronary vasodilation. VI. Detection of coronary artery disease in human beings with intravenous N-13 ammonia and positron computed tomography. *Am J Cardiol.* 1982;49:1197–1207.
4. Muzik O, Paridon SM, Singh TP, Morrow WR, Dayanikli F, Di Carli MF. Quantification of myocardial blood flow and flow reserve in children with a history of Kawasaki disease and normal coronary arteries using positron emission tomography. *J Am Coll Cardiol.* 1996;28:757–762.
5. Hutchins GD, Schwaiger M, Rosenspire KC, Krivokapich J, Schelbert H, Kuhl DE. Noninvasive quantification of regional blood flow in the human heart using N-13 ammonia and dynamic positron emission tomographic imaging. *J Am Coll Cardiol.* 1990;15:1032–1042.
6. Bergmann SR, Fox KA, Rand AL, et al. Quantification of regional myocardial blood flow in vivo with $H_2^{15}O$. *Circulation.* 1984;70:724–733.
7. Schwaiger M, Ziegler S, Nekolla SG. PET/CT: challenge for nuclear cardiology. *J Nucl Med.* 2005;46:1664–1678.
8. Madar I, Ravert HT, Du Y, et al. Characterization of uptake of the new PET imaging compound ^{18}F-fluorobenzyl triphenyl phosphonium in dog myocardium. *J Nucl Med.* 2006;47:1359–1366.
9. Tai YC, Ruangma A, Rowland D, et al. Performance evaluation of the microPET Focus: a third-generation microPET scanner dedicated to animal imaging. *J Nucl Med.* 2005;46:455–463.
10. Laforest R, Longford D, Siegel S, Newport DF, Yap J. Performance evaluation of the microPET-Focus-F120. *IEEE Transactions Nucl Sci.* 2007;54:42–49.
11. Croteau E, Bénard F, Bentourkia M, Rousseau J, Paquette M, Lecomte R. Quantitative myocardial perfusion and coronary reserve in rats with ^{13}N-ammonia and small animal PET: impact of anesthesia and pharmacologic stress agents. *J Nucl Med.* 2004;45:1924–1930.
12. Nekolla SG, Miethaner C, Nguyen N, Ziegler SI, Schwaiger M. Reproducibility of polar map generation and assessment of defect severity and extent assessment in myocardial perfusion imaging using positron emission tomography. *Eur J Nucl Med.* 1998;25:1313–1321.
13. Iida H, Law I, Pakkenberg B, et al. Quantitation of regional cerebral blood flow corrected for partial volume effect using O-15 water and PET. I. Theory, error analysis, and stereologic comparison. *J Cereb Blood Flow Metab.* 2000;20:1237–1251.

14. Kaufmann PA, Gnecchi-Ruscone T, Yap JT, Rimoldi O, Camici PG. Assessment of the reproducibility of baseline and hyperemic myocardial blood flow measurements with ^{15}O-labeled water and PET. *J Nucl Med.* 1999;40:1848–1856.

15. Kaufmann PA, Camici PG. Myocardial blood flow measurement by PET: technical aspects and clinical applications. *J Nucl Med.* 2005;46:75–88.

16. Kuhle WG, Porenta G, Huang SC, et al. Quantification of regional myocardial blood flow using ^{13}N-ammonia and reoriented dynamic positron emission tomographic imaging. *Circulation.* 1992;86:1004–1017.

17. DiCarli M, Czernin J, Hoh CK, et al. Relation among stenosis severity, myocardial blood flow, and flow reserve in patients with coronary artery disease. *Circulation.* 1995;91:1944–1951.

18. Laubenbacher C, Rothley J, Sitomer J, et al. An automated analysis program for the evaluation of cardiac PET studies: initial results in the detection and localization of coronary artery disease using nitrogen-13-ammonia. *J Nucl Med.* 1993;34:968–978.

19. Grover-McKay M, Ratib O, Schwaiger M, et al. Detection of coronary artery disease with positron emission tomography and rubidium 82. *Am Heart J.* 1992;123:646–652.

20. Bateman TM. Cardiac positron emission tomography and the role of adenosine pharmacologic stress. *Am J Cardiol.* 2004;94(2A):19D–26D.

21. Parkash R, deKemp RA, Ruddy TD, et al. Potential utility of rubidium 82 PET quantification in patients with 3-vessel coronary artery disease. *J Nucl Cardiol.* 2004;11:440–449.

22. Stewart RE, Schwaiger M, Molina E, et al. Comparison of rubidium-82 positron emission tomography and thallium-201 SPECT imaging for detection of coronary artery disease. *Am J Cardiol.* 1991;67:1303–1310.

23. Cherednichenko G, Zima AV, Feng W, Schaefer S, Blatter LA, Pessah IN. NADH oxidase activity of rat cardiac sarcoplasmic reticulum regulates calcium-induced calcium release. *Circ Res.* 2004;94:478–486.

24. Schuler F, Casida JE. The insecticide target in the PSST subunit of complex I. *Pest Manag Sci.* 2001;57:932–940.

25. Yu M, Guaraldi MT, Mistry M, et al. BMS-747158-02: a novel PET myocardial perfusion imaging agent. *J Nucl Cardiol.* 2007;14:789–798.

26. Leppo JA, Meerdink DJ. Comparison of the myocardial uptake of a technetium-labeled isonitrile analogue and thallium. *Circ Res.* 1989;65:632–639.

27. Schelbert HR, Phelps ME, Huang SC, et al. N-13 ammonia as an indicator of myocardial blood flow. *Circulation.* 1981;63:1259–1272.

28. Mullani NA, Goldstein RA, Gould KL, et al. Myocardial perfusion with rubidium-82. I. Measurement of extraction fraction and flow with external detectors. *J Nucl Med.* 1983;24:898–906.

29. Herrero P, Kim J, Sharp TL, et al. Assessment of myocardial blood flow using ^{15}O-water and 1-^{11}C-acetate in rats with small-animal PET. *J Nucl Med.* 2006;47:477–485.

30. Meerdink DJ, Leppo JA. Comparison of hypoxia and ouabain effects on the myocardial uptake kinetics of technetium-99m hexakis 2-methoxyisobutyl isonitrile and thallium-201. *J Nucl Med.* 1989;30:1500–1506.